Journal of Sound and Vibration (1999) **227**(1), 65–84
Article No. jsvi.1999.2325, available online at http://www.idealibrary.com on IDEAL®

AUTO-PARAMETRIC RESONANCE IN CYCLINDRICAL SHELLS USING GEOMETRIC AVERAGING

F. A. McRobie and A. A. Popov†

Engineering Department, University of Cambridge, Trumpington Street, Cambridge CB2 1PZ, England

AND

J. M. T. Thompson

Centre for Nonlinear Dynamics and its Applications, University College London, Gower Street, London WC1E 6BT, England

(*Received* 31 *July* 1998, *and in final form* 9 *April* 1999)

A study is presented of internal auto-parametric instabilities in the free non-linear vibrations of a cylindrical shell, focussed on two modes (a concertina mode and a chequerboard mode) whose non-linear interaction breaks the in–out symmetry of the linear vibration theory: the two mode interaction leads to preferred vibration patterns with larger deflection inwards than outwards, and at internal resonance, significant energy transfer occurs between the modes. A Rayleigh–Ritz discretization of the von Kármán–Donnell equations leads to the Hamiltonian and transformation into action-angle co-ordinates followed by averaging provides readily a geometric description of the modal interaction. It was established that the interaction should be most pronounced when there are slightly less than $2\sqrt{N}$ square chequerboard panels circumferentially, where N is the ratio of shell radius to thickness.

1. INTRODUCTION

Internal auto-parametric instabilities of thin vibrating shells can generate significant energy transfer between modes in a manner that cannot be described by linear vibration theory. In this paper, the simplest example of the phenomenon is considered, namely the unforced, undamped vibrations of an infinitely-long circular–cylindrical shell. By applying methods of Hamiltonian dynamical systems theory a simple geometric description is obtained of the interaction phenomenon which can form the basis for further, more pragmatic analysis.

Fundamental studies of cylindrical shells have played a central role in the understanding of static buckling of shells (see e.g. references [1–9]), and such a shell is adopted here as an archetype for the development of the non-linear dynamical

†Former member of the Centre for Nonlinear Dynamics and its Applications, University College London.

0022-460X/99/410065 + 20 $30.00/0

analyses. Original works on non-linear shell vibrations by Evensen [10] and Volmir [11], for example, have more recently been supplemented by modal coupling analyses of Nayfeh and Balachandran [12], Liu [13], Bogdanovich [14], Thompson and de Souza [15], and Popov *et al.* [16]. In this paper, however, rather than employing the traditional approximation methods of engineering mathematics the geometrical interpretation of the averaging method of Hamiltonian dynamical systems theory is applied. Following the pioneering and rigorous theoretical advances of Kolmogorov, Arnol'd and Moser this method has been widely applied in the physics literature, particularly by Chirikov [17]. Although a number of celebrated theorems have been proven involving averaging, some fundamental proofs on the general validity of the method have yet to be supplied. Rather than concentrating upon the rigour of the mathematics, we follow instead the physicists and place our emphasis upon the elegant description of the dynamics that can be obtained.

Following non-linear shell theory, we start with the non-linear von Kármán–Donnell equations for a cylindrical shell and make a Rayleigh–Ritz discretization to the selected modes of transverse deflection. The in-plane equilibrium and compatibility conditions are then exactly satisfied by use of the Airy stress function. Two modes are selected that are known to have significant *static* post-buckling interaction under axial compression. These two modes can combine to break the in–out symmetry of the linear theory, i.e., they give larger deflection inwards than outwards. In the dynamical setting this leads to preferred vibration patterns with larger deflection inwards than outwards. The two modes have concertina (Figure 1(a)) and chequerboard (Figure 1(b)) forms, and the energetically favourable manner in which they can combine is illustrated in the analysis.

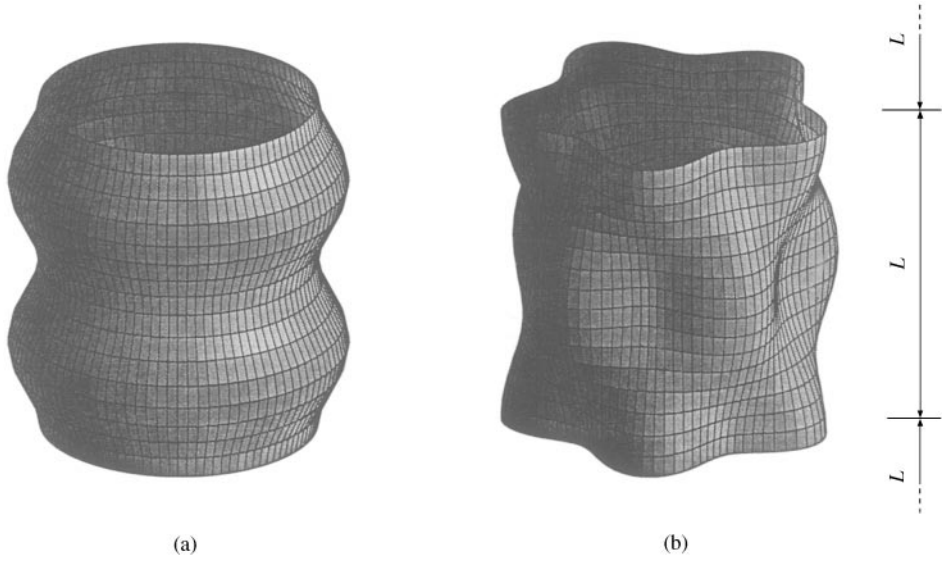

Figure 1. The two vibration modes: (a) concertina; (b) chequerboard.

Hamilton's equations describing the linearized equations are, of course, integrable. By averaging the Hamiltonian at near-resonance conditions another integrable system is obtained, describing approximately the non-linear motions. The final results of this analysis are identical with those of more algebraic approaches of approximation theory, such as the slow-fluctuation method of Augusteijn, Breitenberger and Mueller [18–20], itself a variant of the method of "slowly varying amplitude and phase".

By using our approach, all the non-linear dynamic phenomena that are of practical significance are described: the so-called "dynamic instability regions", the local bifurcation structure and the amplitudes of significant orbits are all readily captured. If desired, complete solution by quadrature for the general, quasi-periodic motions using Jacobian elliptic functions is also possible, as with the more traditional approaches. This more modern description, however, is better placed for future development to describe either the minutiae of chaotic interactions present even in the two-mode free-vibration case, or the complex many-mode interactions in the forced, damped case.

A strong analogy is demonstrated between the modal interaction of this shell and the interaction between the vertical and pendulum modes of a simple spring pendulum, whose internal resonance phenomena have been widely studied (see, e.g., references [21–23]). The concertina mode is analogous to vertical oscillations and the chequerboard mode to pendulum-like motions, and in the following we shall therefore look in particular at the loss of stability of pure concertina motions. However, this analogy is far from obvious and it is a result of the rigorous analysis presented.

2. THE SHELL MODEL

2.1 VON KÁRMÁN–DONNELL EQUATIONS FOR A CYLINDRICAL SHELL

We consider here the free oscillations of an infinitely long circular–cylindrical shell, looking at the interaction between two spatially periodic modes of vibration. We use a formulation similar to that of one earlier work on the flexural oscillations of cylindrical shells that are parametrically excited by axial forcing [16].

The non-linear free vibrations of a thin cylindrical shell are described by a system of two coupled partial differential equations in the form

$$\rho h \frac{\partial^2 w}{\partial t^2} + D\Delta^2 w = \frac{1}{R}\frac{\partial^2 \Phi}{\partial x^2} + [\Phi, w], \tag{1}$$

$$\frac{1}{\mathrm{E}h}\Delta^2 \Phi = -\frac{1}{R}\frac{\partial^2 w}{\partial x^2} - \frac{1}{2}[w, w], \tag{2}$$

where

$$[f, g] = \frac{\partial^2 f}{\partial x^2}\frac{\partial^2 g}{\partial y^2} - 2\frac{\partial^2 f}{\partial x \partial y}\frac{\partial^2 g}{\partial x \partial y} + \frac{\partial^2 f}{\partial y^2}\frac{\partial^2 g}{\partial x^2}.$$

Here, x is the axial length co-ordinate, y the circumferential length co-ordinate, t the time, R the radius of the cylinder, h the shell thickness, w the normal displacement (positive inwards), Φ the in-plane (Airy) stress function, and Δ^2 is the biharmonic operator. The material is elastic and isotropic: E is Young's modulus, v Poisson's ratio, ρ the mass density, and $D = Eh^3/12(1 - v^2)$ is the bending stiffness of the shell.

These governing PDEs are of quasi-linear hyperbolic type. The system was introduced by von Kármán in 1910 for plates, i.e., without the terms depending on the radius R. Subsequently, in 1933, Donnell suggested (1) and (2) for shallow shell problems: they are adequate for the periodic modes of the cylinder considered here. Notice that although we later use an energy approach, we shall need equation (2) to derive the in-plane stresses in terms of the assumed radial displacement $w(x, y, t)$.

2.2. RAYLEIGH–RITZ DISCRETIZATION PROCEDURE

There are several methods for approximating PDEs by finite-dimensional systems of ODEs such as the Rayleigh–Ritz method, Galerkin projection, finite differences, finite and boundary element methods. In this paper we adopt the former.

Initially, we consider lateral deflections w of the form [24]

$$w(x, y, t) = \sum_{k=0}^{\infty} \sum_{n=0}^{\infty} q_{kn}(t) h \cos\left(\frac{k\pi x}{L}\right) \cos\left(\frac{ny}{R}\right) \tag{3}$$

before specializing this to the two-mode case with two carefully chosen modes which together give a spatially periodic pattern of axial wavelength $2L$.

The total potential energy V of the shell is, in this case, the sum of the strain energies U_s of stretching and U_b of bending. Over an axial half-wavelength, these can be written as

$$U_s = \frac{1}{2Eh} \int_0^L \int_0^{2\pi R} \{(\Delta\Phi)^2 - (1 + v)[\Phi, \Phi]\} \, \mathrm{d}x \, \mathrm{d}y, \tag{4}$$

$$U_b = \frac{D}{2} \int_0^L \int_0^{2\pi R} \{(\Delta w)^2 - (1 - v)[w, w]\} \, \mathrm{d}x \, \mathrm{d}y, \tag{5}$$

where Δ is the Laplace operator, while the kinetic energy of an oscillation is (by this shell theory)

$$T = \frac{1}{2} \int_0^L \int_0^{2\pi R} \rho h \left(\frac{\partial w}{\partial t}\right)^2 \mathrm{d}x \, \mathrm{d}y. \tag{6}$$

Substituting the assumed form of the lateral deflections (3) into the right-hand side of equation (2) one may solve for the stress-function Φ as a particular solution Φ_{par}. Expressing Φ in terms of $q_i(t)$ $(i = 0, 1, 2, \ldots)$, one may then evaluate the total energy using integrals (4)–(6). One can usefully perform all of these calculations by means of general computer algebra routines.

2.3. ENERGY FUNCTIONS FOR TWO INTERACTING MODES

Specializing to the two-mode case, we adopt the approximation function

$$w(x, y, t) = q_1(t)h\cos\left(\frac{\pi x}{L}\right)\cos\left(\frac{ny}{R}\right) + q_2(t)h\cos\left(\frac{2\pi x}{L}\right). \tag{7}$$

These two modes are known to have an important non-linear interaction in the post-buckling of axially compressed cylinders [7]. The former is the chequerboard mode with $2n$ panels circumferentially and 2 panels axially in a wavelength $2L$; see Figure 1(b) for $n = 5$. The latter is the concertina mode with axial wavelength L; see Figure 1(a). The wavelengths and spatial phases are such that along alternate hoops of maximum amplitude of the concertina mode the chequerboard mode has alternately maximum or zero amplitude. Taken together the two modes can break the in–out symmetry exhibited by each individually. This is illustrated in Figure 2 for mode coupling with two different values of the total potential energy. This asymmetry is discernible in the total potential energy function, see Figure 3(a), of the non-linear shell theory. In the subsequent analysis this manifests itself in the form of vibrations having greater amplitudes inwards than outwards.

The corresponding potential energy function can be written as

$$V = \tfrac{1}{2}k_{11}q_1^2 + \tfrac{1}{2}k_{22}q_2^2 + \tfrac{1}{2}k_{112}q_1^2q_2 + \tfrac{1}{24}k_{1111}q_1^4 + \tfrac{1}{4}k_{1122}q_1^2q_2^2. \tag{8}$$

The above finite expansion for the potential function is exact within the basic shallow-shell theory employed, the coefficients being given by

$$\frac{k_{11}}{V_c} = \frac{8\alpha^2}{\pi^2(1+\gamma^2)^2} + \frac{2\pi^2\beta^4(1+\gamma^2)^2}{3(1-\nu^2)}, \quad \frac{k_{22}}{V_c} = \frac{16\alpha^2}{\pi^2} + \frac{64\pi^2\beta^4}{3(1-\nu^2)},$$

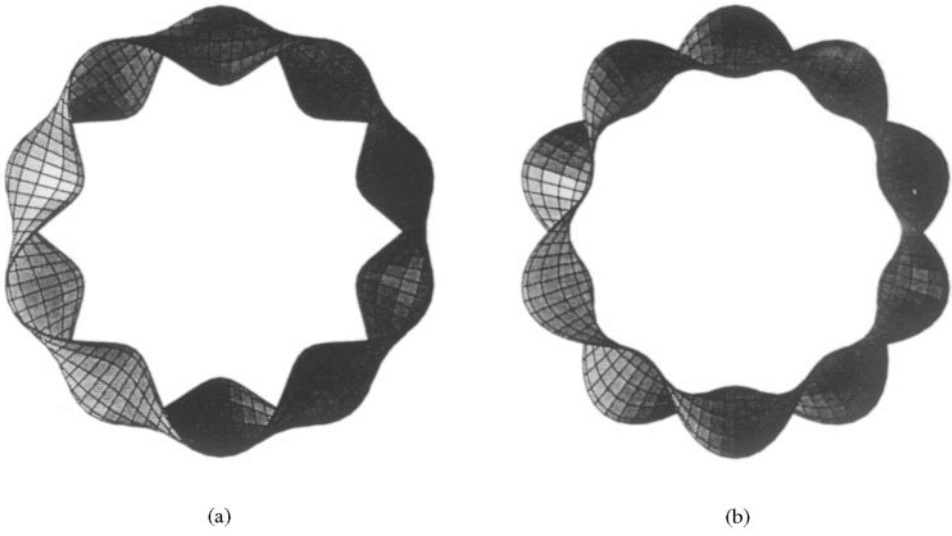

Figure 2. Mode shapes for two different values of the total potential energy function: (a) state A; (b) state B in Figure 3.

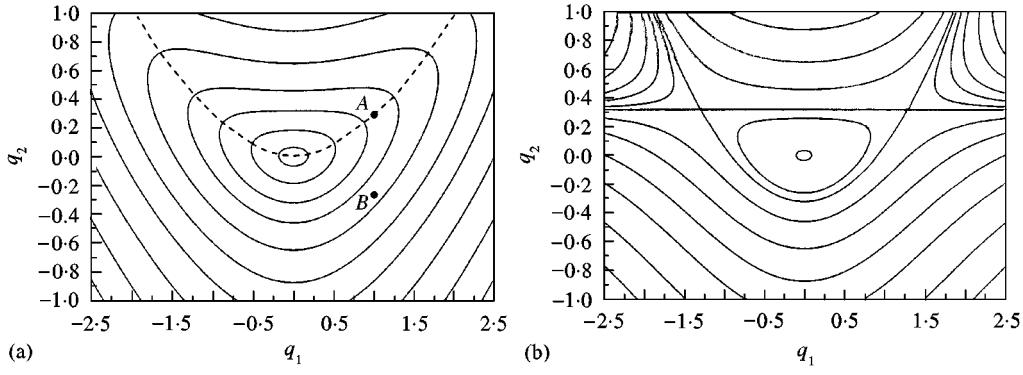

Figure 3. Potential energy contours for the two degree-of-freedom model: (a) the complete non-linear function $V(q_1, q_2)$; (b) the same function truncated to cubic terms.

$$\frac{k_{112}}{V_c} = -4\alpha\beta^2\gamma^2\left(1 + \frac{8}{(1+\gamma^2)^2}\right), \quad \frac{k_{1111}}{V_c} = 3\pi^2\beta^4(1+\gamma^4),$$

$$\frac{k_{1122}}{V_c} = 64\pi^2\beta^4\gamma^4\left[\frac{1}{(1+\gamma^2)^2} + \frac{1}{(9+\gamma^2)^2}\right],$$

where

$$V_c = \pi^3 \mathrm{E}hRL/16, \quad \alpha = \mathrm{h/R}, \quad \beta = \mathrm{h/L} \quad \text{and} \quad \gamma = Ln/\pi R,$$

the latter being the aspect ratio of the panels of the chequerboard mode.

The kinetic energy is

$$T = \tfrac{1}{2}m_1\dot{q}_1^2 + \tfrac{1}{2}m_2\dot{q}_2^2, \tag{9}$$

where

$$m_1 = \tfrac{1}{2}\pi\rho h^3 RL \quad \text{and} \quad m_2 = \pi\rho h^3 RL. \tag{10}$$

2.4. LINEAR FREQUENCIES AND INTERNAL RESONANCE

Each term in the series (3) is an eigenfunction of the linearized shell equations. The corresponding eigenvalues are

$$\omega_{(k,n)} = \sqrt{\frac{E}{\rho}}\frac{1}{R}\left\{\frac{\alpha^2}{12(1-\nu^2)}S^4(1+\Lambda^2)^2 + \frac{1}{(1+\Lambda^2)^2}\right\}^{1/2}, \tag{11}$$

where $S = k\pi R/L$ is a non-dimensional measure of (the reciprocal of) the axial wavelength $2L/k$ (and the chequerboard panel aspect ratio $\Lambda = n/S$).

2.5. COUPLED LOW-ENERGY DEFORMATIONS BREAKING IN–OUT SYMMETRY

Typical potential energy contours of the complete non-linear function $V(q_1, q_2)$ are shown in Figure 3. Notice that the shell can minimize its potential energy by deforming along the dashed valley floor along which q_2 varies parabolically with q_1. In this energetically favourable valley, the modes combine to give a shape that has greater inwards than outwards amplitude as illustrated in Figure 4. The curves

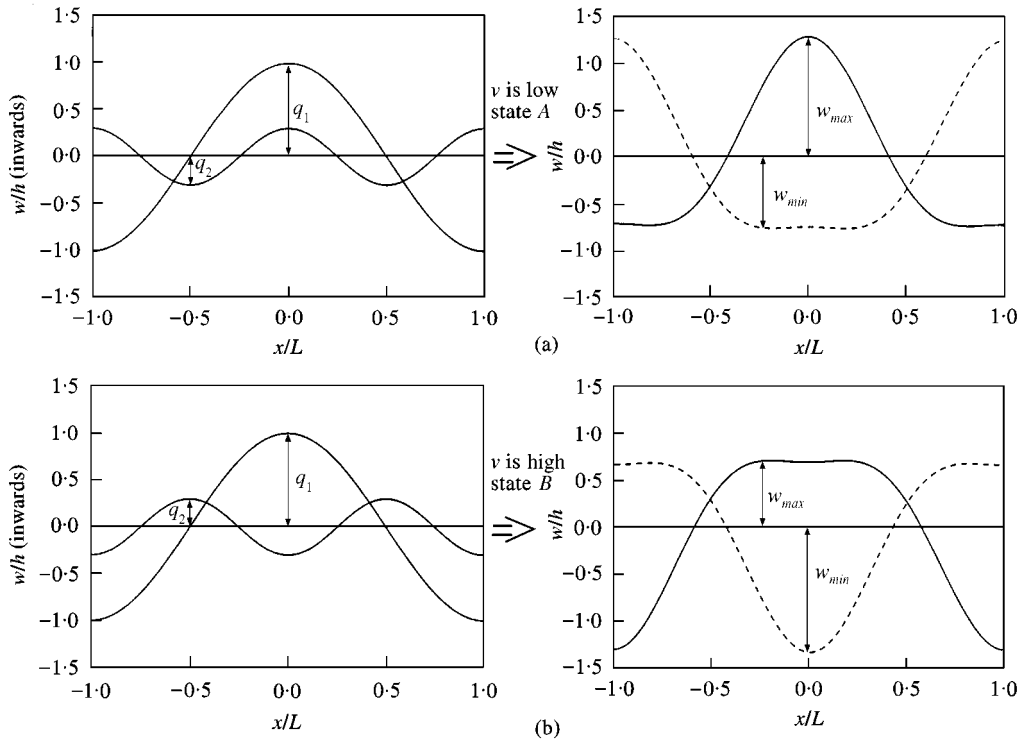

Figure 4. Energetically favourable and unfavourable shapes with equal q_1 but reversed q_2, corresponding to points A and B in Figure 3 at $y = 0$: (a) $q_1 = 1{\cdot}0$ and $q_2 = 0{\cdot}3$ at A; (b) $q_1 = 1{\cdot}0$ and $q_2 = -0{\cdot}3$ at B.

in the second column in Figure 4 show the possible mode shapes separated by a half a period in time. The corresponding mode shapes are shown in Figure 2.

We shall see later that the employed perturbation method only makes use of the cubic energy terms. With only the cubic terms, the potential energy function has the form of Figure 3(b). In the vicinity of the trivial equilibrium solution the two pictures are of course in close aggreement. For absolute values of the generalized displacements in the first mode q_1 up to values equal to the thickness of the shell, $q_1 = 1$, the potential energy contours are essentially the same. Notice, however, the invalid saddle solutions that are generated by the truncation to the cubic terms. The perturbation analysis that follows is therefore only valid for amplitudes below the region of these saddles.

3. THE DYNAMICS

3.1. THE HAMILTONIAN

Upon writing the momenta $p_1 \equiv m_1\dot{q}_1$, $p_2 \equiv m_2\dot{q}_2$ conjugate to the displacements q_1, q_2, the Hamiltonian of our two degree-of-freedom model is

$$H = \frac{1}{2}\frac{p_1^2}{m_1} + \frac{1}{2}\frac{p_2^2}{m_2} + \frac{1}{2}m_1\omega_1^2 q_1^2 + \tfrac{1}{2}m_2\omega_2^2 q_2^2 + H_1(q_1, q_2), \tag{12}$$

where $\omega_1 \equiv \omega_{(1,n)}$ and $\omega_2 \equiv \omega_{(2,0)}$ are the natural frequencies of the chequerboard and concertina modes, respectively, as given by equation (11). The function $H_1(q_1, q_2)$ contains the non-linear coupling terms:

$$H_1 = \tfrac{1}{2}k_{112}q_1^2q_2 + \tfrac{1}{24}k_{1111}q_1^4 + \tfrac{1}{4}k_{1122}q_1^2q_2^2. \tag{13}$$

Hamilton's equations can be readily obtained from the Hamiltonian function as usual, giving the time-derivatives $(\dot{\mathbf{p}}, \dot{\mathbf{q}})$ as non-linear functions of the conjugate co-ordinates $\mathbf{q}$ and momenta $\mathbf{p}$. We do not state these equations here, pursuing instead a perturbation analysis. The method used is that of averaging, and we follow the geometric interpretation of the method described by Berry [25] and Chirikov [17].

3.2. ACTION-ANGLE CO-ORDINATES

The well-known canonical (symplectic) transformation [26] and its inverse

$$q_i = \sqrt{\frac{2I_i}{m_i\omega_i}}\cos\theta_i, \quad p_i = -\sqrt{2m_i\omega_iI_i}\sin\theta_i, \tag{14}$$

$$I_i = \frac{p_i^2}{2m_i\omega_i} + \frac{m_i\omega_iq_i^2}{2}, \quad \theta_i = \tan^{-1}(-p_i/m_i\omega_iq_i), \tag{15}$$

transforms the original variables $(\mathbf{p}, \mathbf{q})$ into action-angle co-ordinates $(\mathbf{I}, \boldsymbol{\theta})$. The actions I_i and angles θ_i are expressed in terms of amplitudes A_i (always $A_i \geqslant 0$) and phases β_i by using

$$I_i = \tfrac{1}{2}m_i\omega_iA_i^2 \quad \text{and} \quad \theta_i = \omega_it + \beta_i, \tag{16}$$

and it follows that

$$q_i = A_i\cos(\omega_it + \beta_i), \tag{17}$$

$$p_i = -m_i\omega_iA_i\sin(\omega_it + \beta_i). \tag{18}$$

For the linear system, equations (17) and (18) are the normal modes of vibration, but for the non-linear system the amplitudes A_i and phases β_i are no longer constant in time.

After applying the canonical transformation (14), the Hamiltonian (12) becomes

$$H = I_1\omega_1 + I_2\omega_2 + 4bI_1\sqrt{I_2}\cos^2\theta_1\cos\theta_2 + 4cI_1^2\cos^4\theta_1 + 4dI_1I_2\cos^2\theta_1\cos^2\theta_2, \tag{19}$$

where

$$b = \frac{k_{112}}{2m_1\omega_1\sqrt{2m_2\omega_2}}, \quad c = \frac{k_{1111}}{24m_1^2\omega_1^2}, \quad d = \frac{k_{1122}}{4m_1\omega_1m_2\omega_2}.$$

Upon expressing the final terms (which are functions of the θ's) as a Fourier series, the Hamiltonian may be written as

$$H = H_0 + H_1 = \mathbf{I}.\boldsymbol{\omega} + \sum H_{1mj}(\mathbf{I})e^{\mathbf{i}m_j\boldsymbol{\theta}}, \tag{20}$$

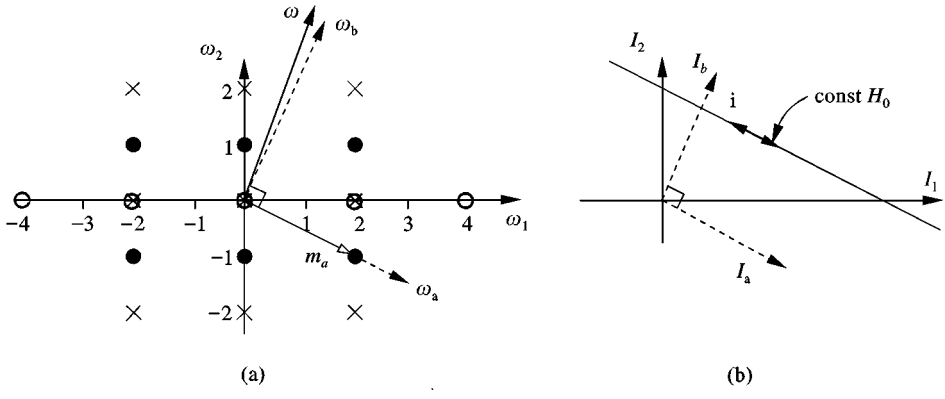

Figure 5(a). The lattice of integers for the Fourier series: ● $\cos^2\theta_1\cos\theta_2$; ○ $\cos^4\theta_1$; $\times\cos^2\theta_1\cos^2\theta_2$. The shell frequencies $\boldsymbol{\omega} = (\omega_1, \omega_2)^{\mathrm{T}}$ are nearly orthogonal to the lattice vector $\mathbf{m}_a = (2, -1)^{\mathrm{T}}$; (b) the **I**-plane, showing the change of action $\dot{\mathbf{I}}$ on the plane of constant H_0 parallel to $\mathbf{m}_a$.

where $H_0 \equiv \mathbf{I}.\boldsymbol{\omega}$ is the Hamiltonian function of the linear system and $\{\mathbf{m}_j\}$ is an integer lattice. (Here and in what follows the vector notations $\mathbf{I} = (\mathrm{I}_1, \mathrm{I}_2)^{\mathrm{T}}$, $\boldsymbol{\omega} = (\omega_1, \omega_2)^{\mathrm{T}}$, $\boldsymbol{\theta} = (\theta_1, \theta_2)^{\mathrm{T}}$ and $\boldsymbol{\beta} = (\beta_1, \beta_2)^{\mathrm{T}}$, are used.) In equation (19) the elements of $\{\mathbf{m}_j\}$ are readily obtained by expanding the products of cosines:

$$\cos^2\theta_1\cos\theta_2 = \tfrac{1}{2}\cos\theta_2 + \tfrac{1}{4}\cos(2\theta_1 + \theta_2) + \tfrac{1}{4}\cos(2\theta_1 - \theta_2),$$

$$\cos^4\theta_1 = \tfrac{3}{8} + \tfrac{1}{2}\cos 2\theta_1 + \tfrac{1}{8}\cos 4\theta_1,$$

$$\cos^2\theta_1\cos^2\theta_2 = \tfrac{1}{4} + \tfrac{1}{4}\cos 2\theta_1 + \tfrac{1}{4}\cos 2\theta_2 + \tfrac{1}{8}\cos(2\theta_1 + 2\theta_2) + \tfrac{1}{8}\cos(2\theta_1 - 2\theta_2).$$

The points in the corresponding integer lattice are shown in Figure 5(a).

For a given shell, the linear natural frequencies are constants, written as the vector $\boldsymbol{\omega}$. For internal resonance, one seeks an integer vector $\mathbf{m}_a$ from the lattice $\{\mathbf{m}_j\}$ that is almost orthogonal to $\boldsymbol{\omega}$, i.e.,

$$\mathbf{m}_a.\boldsymbol{\omega} = \varepsilon, \quad |\varepsilon| \ll \|\omega\|. \tag{21}$$

This is illustrated in Figure 5(a). Since the elements of ω are naturally positive, the nearly orthogonal vector $\mathbf{m}_a$ must lie in the upper-left or lower-right quadrants. For our lattice, we have the possible (two-frequency) resonance conditions

$$\mathbf{m}_a = \pm(2, -1)^{\mathrm{T}} \quad \text{or} \quad \pm(1, -1)^{\mathrm{T}}. \tag{22}$$

We shall investigate the former, assuming that the shell properties are such that

$$2\omega_1 - \omega_2 = \varepsilon. \tag{23}$$

3.3. AVERAGING

The Hamiltonian is now averaged over a certain time-scale to obtain an approximate Hamiltonian which should describe the motions over this time-scale. The time-scale for averaging is chosen to be sufficiently long that the high-frequency non-resonant terms of (frequency $\mathbf{m}_j.\boldsymbol{\omega}$ $(j \neq a)$) average to close to

zero, but short enough that the slowly varying actions $\mathbf{I}$, phases β and the term $e^{i\varepsilon t}$ may be assumed constant over the averaging interval.

Up to a constant, this gives the averaged Hamiltonian

$$\bar{H} = \mathbf{I} \,.\, \boldsymbol{\omega} + \bar{H}_1 \tag{24}$$

where

$$\bar{H}_1 = \bar{H}_{1ma}(\mathbf{I}) \cos \theta_a \quad \text{and} \quad \theta_a = \mathbf{m}_a \,.\, \boldsymbol{\theta}. \tag{25}$$

In our system, the function $\bar{H}_{1ma}(\mathbf{I}) = bI_1\sqrt{I_2}$, this being the coefficient of the resonant $\cos(2\theta_1 - \theta_2)$ term.

All further analysis gives only an approximation to the true system dynamics. However, the averaged Hamiltonian $\bar{H}$ describes exactly the motions of a "nearby" system. It is this nearby system that we proceed to study, and this nearby system is integrable.

As usual in Hamiltonian dynamical systems theory, before attempting to solve any equation, we proceed to make transformations to obtain the simplest possible statement of the problem. We now choose a rotated co-ordinate system with an action I_a parallel to $\mathbf{m}_a$, and the remaining action I_b in a direction $\mathbf{m}_b$ perpendicular to this (see Figure 5(b)).

We have chosen to study the resonance associated with $\mathbf{m}_a = (2, -1)^{\mathrm{T}}$, and now choose the orthogonal direction $\mathbf{m}_b = (1, 2)^{\mathrm{T}}$. (If more than two modes were involved in this resonance, we would need to select a mutually orthogonal set of such vectors $\{\mathbf{m}_b\}$, each orthogonal to $\mathbf{m}_a$).

A little care is needed with the rotation to the new co-ordinates, since $\mathbf{m}_a$ and $\mathbf{m}_b$ are not of unit magnitude. Using the transformation

$$B = \begin{pmatrix} [\mathbf{m}_a]^{\mathrm{T}} \\ [\mathbf{m}_b]^{\mathrm{T}} \end{pmatrix} = \begin{pmatrix} 2 & -1 \\ 1 & 2 \end{pmatrix}, \tag{26}$$

and defining

$$(\theta_a, \theta_b)^{\mathrm{T}} \equiv \boldsymbol{\phi} \equiv B\boldsymbol{\theta}, \; (I_a, I_b)^{\mathrm{T}} \equiv \mathbf{J} \equiv B^{-T}\mathbf{I}, \; (\omega_a, \omega_b)^{\mathrm{T}} \equiv \boldsymbol{\Omega} \equiv B\omega, \tag{27–29}$$

we obtain the Hamiltonian in terms of the rotated co-ordinates $(\mathbf{J}, \phi)$ as

$$\bar{H}(\mathbf{J}, \boldsymbol{\phi}) = \mathbf{J} \,.\, \boldsymbol{\Omega} + \bar{H}_{1ma}(\mathbf{J}) \cos \theta_a. \tag{30}$$

(That this transformation is canonical, with $\mathbf{J}$, $\boldsymbol{\phi}$ conjugate, can be shown by using the standard theory of generating functions (see, e.g., reference [27]), with generating functions $S_1(\mathbf{Q}, \boldsymbol{\theta}) = \mathbf{Q} \,.\, B\boldsymbol{\theta}$ and $S_2(\boldsymbol{\phi}, \mathbf{Q}) = -\boldsymbol{\phi} \,.\, \mathbf{Q}$)

In the rotated co-ordinates, $\bar{H}(\mathbf{J}, \boldsymbol{\phi}) = \bar{H}(I_a, I_b, \theta_a)$ which is independent of the co-ordinate θ_b (i.e., is "cyclic" in θ_b), thus

$$\dot{I}_b = -\partial \bar{H}/\partial \theta_b = 0, \tag{31}$$

and hence the action I_b is a constant of the motion. Along with the original constant $\bar{H}$ one now has enough constants to integrate the (approximate) system.

Geometrically, the result $\dot{I}_b = \mathbf{m}_b \,.\, \dot{\mathbf{I}}/|\mathbf{m}_b|^2 = 0$ states that $\dot{\mathbf{I}}$ is perpendicular to (all the) $\mathbf{m}_b$ and is thus parallel to $\mathbf{m}_a$ (see Figure 5(b)). From any given initial condition $\mathbf{I}$, it follows that the action of all subsequent motion lie along the line through $\mathbf{I}$-space

parallel to $\mathbf{m}_a$. Since the components of $\mathbf{I}$ are necessarily positive, all subsequent actions lie on the segment on this line passing through the positive quadrant.

The Hamiltonian of the linear system is thus

$$H_0 = \mathbf{I}.\boldsymbol{\omega} = \mathbf{J}.\boldsymbol{\Omega} = I_a\varepsilon + I_b\omega_b, \tag{32}$$

of which the final term is a constant.

3.3.1. *Perfect resonance*

At the conditions of perfect resonance ($\varepsilon = 0$), one obtains from equation (32) that $H_0 = I_b\omega_b$ which is constant. The Hamiltonian H_0 of the linear system is thus a conserved quantity of the (approximate) non-linear system at the conditions of perfect resonance. Since $\bar{H} = H_0 + \bar{H}_1$, then so also is $\bar{H}_1$. Geometrically, these results state that, in $\mathbf{I}$-space, any line parallel to $\mathbf{m}_a$ is a line of constant H_0.

Since I_b is constant, its value is determined once and for all by the initial conditions. Evolution in $\mathbf{I}$-space proceeds along the direction parallel to $\mathbf{m}_a$, parameterized by the single co-ordinate I_a.

The function $\bar{H}_{1ma}(\mathbf{I})$ may thus be expressed as a function of I_a only, giving

$$\bar{H} = \bar{H}(I_a, \theta_a) = H_0 + \bar{H}_{1ma}(I_a)\cos\theta_a. \tag{33}$$

The trajectories of this system fill the (I_a, θ_a) plane. These trajectories are level sets of the function $\bar{H}_{1ma}(I_a)\cos\theta_a$, easily obtained numerically by plotting contours over the (I_a, θ_a) plane, as illustrated in Figure 6.

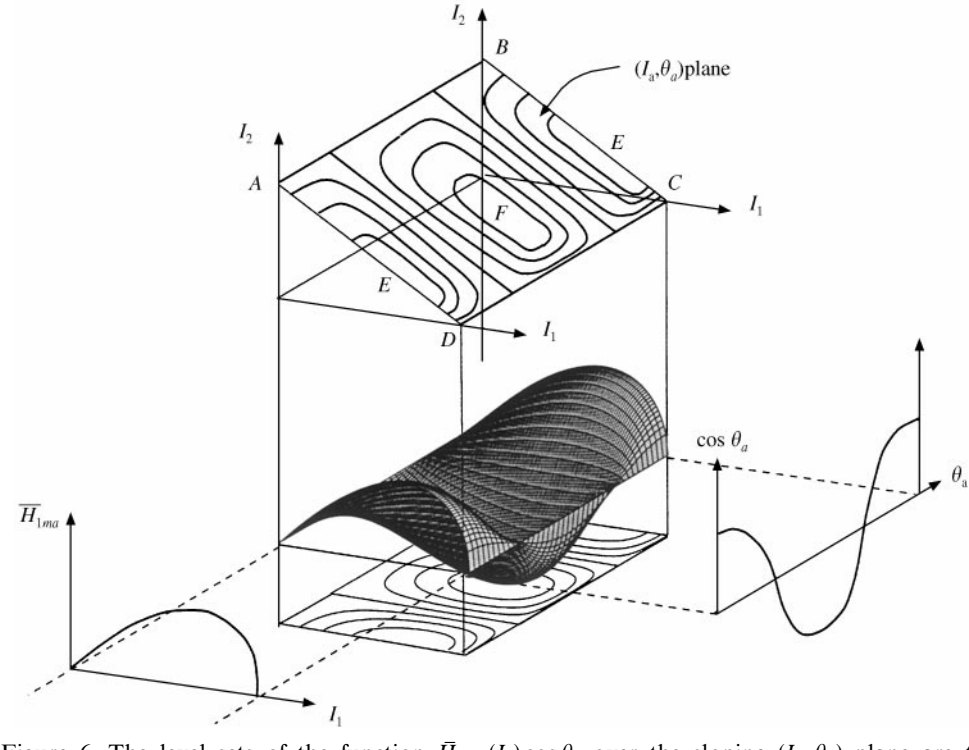

Figure 6. The level sets of the function $\bar{H}_{1ma}(I_a)\cos\theta_a$ over the sloping (I_a, θ_a) plane are the trajectories at resonance.

Note that the function $\bar{H}_{1ma}(I_a) = bI_1\sqrt{I_2}$ is linearly sloping at the $I_1 = 0$ end, but has infinite slope at the $I_2 = 0$ end, due to the square root.

A general contour on the (I_a, θ_a) plane is a closed loop, and corresponds to a quasi-periodic motion. Continued application of the Hamiltonian systems methodology would now have transformed the system yet again, by using another generating function, into a pair of action-angle co-ordinates describing the motion around these closed loops on the (I_a, θ_a) plane, with the action constant on each trajectory. We shall not proceed with this, as the system of equations are already simple enough to integrate explicitly.

Since

$$\dot{I}_a = -\partial\bar{H}/\partial\theta_a = \bar{H}_{1ma}\sin\theta_a, \tag{34}$$

then eliminating θ_a by using equations (25) gives

$$\dot{I}_a = \pm\sqrt{\bar{H}_{1ma}^2 - \bar{H}_1^2}, \tag{35}$$

whence

$$\pm\, \mathrm{d}I_a/\sqrt{\bar{H}_{1ma}^2(I_a) - \bar{H}_1^2} = \mathrm{d}t. \tag{36}$$

The denominator on the left is the square root of a cubic polynomial in I_a and integration is straightforward, by using Jacobian elliptic functions. However, rather than presenting lengthy algebraic expressions for the general quasi-periodic motions [20], it is more instructive to extract a qualitative understanding from the geometric description that we have developed, such that a number of important quantitative results can then be achieved rather painlessly.

To obtain a more familiar picture, consider a set of orbits of equal constant linear energy H_0 with a Poincaré section defined by the plane of points $(q_1, -p_1/m_1\omega_1)$ sampled when $p_2 = 0$, $q_2 > 0$. This is illustrated in Figure 7(b). (Plotting orbits of equal total energy $\bar{H}$ may be more usual, but if the displacements are small, $H_0 \gg \bar{H}_1$ and so $H_0 \approx \bar{H}$, and the pictures are substantially similar). Note that the Cartesian plane $(q_1, -p_1/m_1\omega_1)$ is also parameterized in polar co-ordinates by (A_1, θ_1), by using equations (17) and (18).

When $p_2 = 0$, (with $q_2 > 0$) equation (18) gives $\theta_2 = 0$ thus on the Poincaré section, $\theta_1 = \theta_a/2$. There is thus a one-to-two mapping of the (I_a, θ_a) plane onto the $(q_1, -p_1/m_1\omega_1)$ plane. The upper horizontal edge of the (I_a, θ_a) plane (line AB of Figures 6 and 7(a)), having $I_1 = 0$ (and thus $A_1 = 0$) maps to the origin of the $(q_1, -p_1/m_1\omega_1)$ plane. The lower horizontal edge (line DC, Figures 6 and 7(a)) has $I_2 = 0$, thus $\bar{H} = H_0 = I_1\omega_1$. This lower horizontal edge thus maps to the circle of radius $A_1 = \sqrt{2I_1/m_1\omega_1} = \sqrt{2\bar{H}/m_1\omega_1^2}$. If the system is started from initial conditions $(q_1, q_2, p_1, p_2) = (0, q_2^0, 0, 0)$, then $\bar{H} = \frac{1}{2}m_2\omega_2^2 q_2^{0^2}$. The pure q_2 motion is unstable, and the system will fall off down one of the unstable manifolds emanating from the origin at 45°, experiencing a maximum q_1 amplitude of $A_{1,\max} = 2\sqrt{m_2/m_1}\, q_2^0 = 2\sqrt{2}q_2^0$ at the outermost circle.

The points E and F on the (I_a, θ_a) plane correspond to periodic orbits. These lie on the lines $\theta_a = 0, \pi$ and correspond to the condition where $\mathrm{d}\bar{H}_{1ma}/\mathrm{d}I_a = 0$. Since $\bar{H}_{1ma} = bI_1\sqrt{I_2}$ with $I_1 = 2I_a + I_b$, $I_2 = -I_a + 2I_b$, elementary algebra rapidly

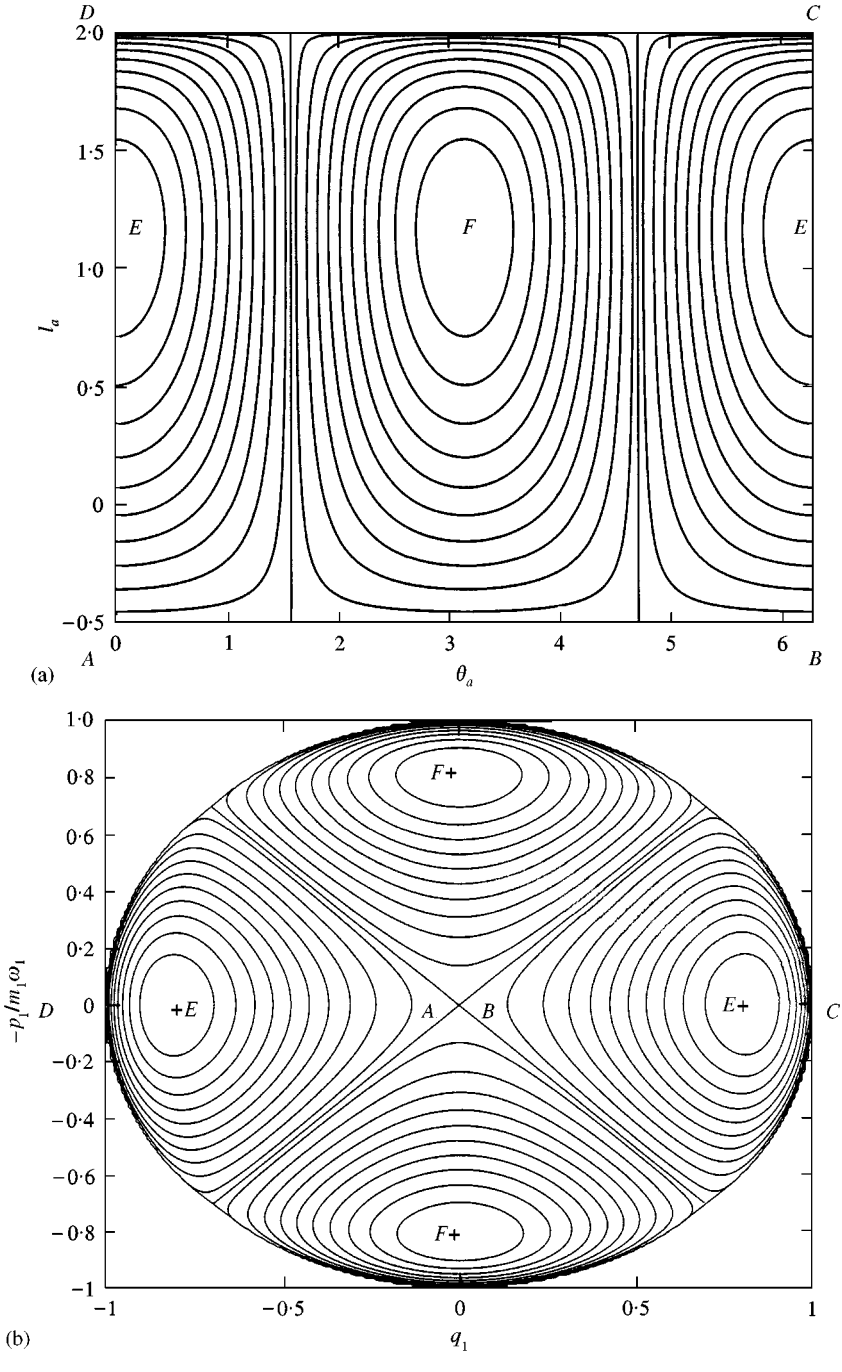

Figure 7. (a). The trajectories on the (I_a, θ_a) plane at resonance; (b) the corresponding trajectories on the $(q_1, -p_1/m_1\omega_1)$ Poincaré plane.

gives $6I_a = 7I_b$, and $I_1 = 4I_2$. Using the approximation that for small vibrations, $\bar{H} \approx H_0 = I_1\omega_1 + I_2\omega_2$ leads to estimates of the periodic orbits as $q_1 = A_1 \cos \omega_1 t$, $q_2 = \frac{1}{4}A_1 \cos 2\omega_1 t$, with the constant amplitude $A_1 = \sqrt{\frac{2}{3}}A_{1,\max}$ (i.e., with

a maximum q_1 amplitude equal to a fraction 0.82 of its maximum homoclinic amplitude).

Recalling the analogy with the oscillations of a spring pendulum indicates that the periodic orbits E and F correspond to the familiar, periodic "cup" and "cap" motions of the pendulum, which involve both vertical and horizontal oscillations. Note, however, that the difference in modal masses for the shell vibrations leads to a ratio of chequerboard to concertina amplitudes of 4, rather than the ratio of 2 for the horizontal to vertical amplitudes in the spring pendulum.

3.3.2. *Near resonance*

For the near-resonance case $\varepsilon \neq 0$, we now have $H_0 = I_a\varepsilon + I_b\omega_b$but $\bar{H}_1 = \bar{H}_{1ma}(\mathbf{I})\cos\theta_a$ still. Since the angle(s) θ_b are still cyclic, then $\dot{I}_b = 0$ again, thus the I_bs are again conserved quantities, and there are enough constants of the motion to integrate the system. Since $H_0 = I_a\varepsilon + I_b\omega_b$, of which only the last term is constant, the Hamiltonian of the linear system is not a conserved quantity of the (approximate) non-linear system away from resonance. However, since $I_b\omega_b$ and $\bar{H}$ are constants, the function $\varepsilon I_a + \bar{H}_{1ma}(\mathbf{I})\cos\theta_a$ is a constant. We can thus examine the dynamics by considering level sets of this function over the (I_a, θ_a) plane, (or, alternatively, transformed to the $(q_1, -p_1/m_1\omega_1)$ Poincaré plane again).

The effect of the additive linear terms εI_a on the orbit structure is immediately evident. The stationary points E and F on the $\theta_a = 0$ and π axes move. One moves towards the line AB (where $I_1 = 0$) and the other towards the line CD (where $I_2 = 0$), the direction of movement depending upon the sign of ε. This is illustrated in Figure 8 for $\varepsilon < 0$. For sufficiently large $|\varepsilon|$, one of the stationary points can collide with the line AB. This occurs when

$$|\varepsilon| = \mathrm{d}\bar{H}_{1ma}(I_a)/\mathrm{d}I_a|_{I_1=0} \tag{37}$$

i.e., when the slope of the function $\bar{H}_{1ma}$ at the left-hand end is cancelled by the slope ε of the additive linear term. Since

$$\bar{H}_{1ma} = bI_1\sqrt{I_2} = b(2I_a + I_b)\sqrt{-I_a + 2I_b}, \tag{38}$$

then differentiation with respect to I_a at constant I_b, evaluated at $I_1 = 0$, gives the bifurcation criterion:

$$\varepsilon_{bif} = 2b\sqrt{I_2|_{I_1=0}} = 2b\sqrt{\bar{H}/\omega_2}. \tag{39}$$

If the system is started from the initial condition $(q_1, q_2, p_1, p_2) = (0, q_2^0, 0, 0)$, this criterion may be written as

$$q_2^0 = \left(2 - \frac{\omega_2}{\omega_1}\right)\frac{2m_1\omega_1^2}{k_{112}}. \tag{40}$$

This criterion delineates the limits of the so-called "dynamic instability regions", and we consider the extent of these in section 4.

However, before determining the stability boundaries, we shall extract the bifurcation diagram for these instability regions by obtaining an analytical expression for the (approximate) amplitude of the periodic orbits. The periodic

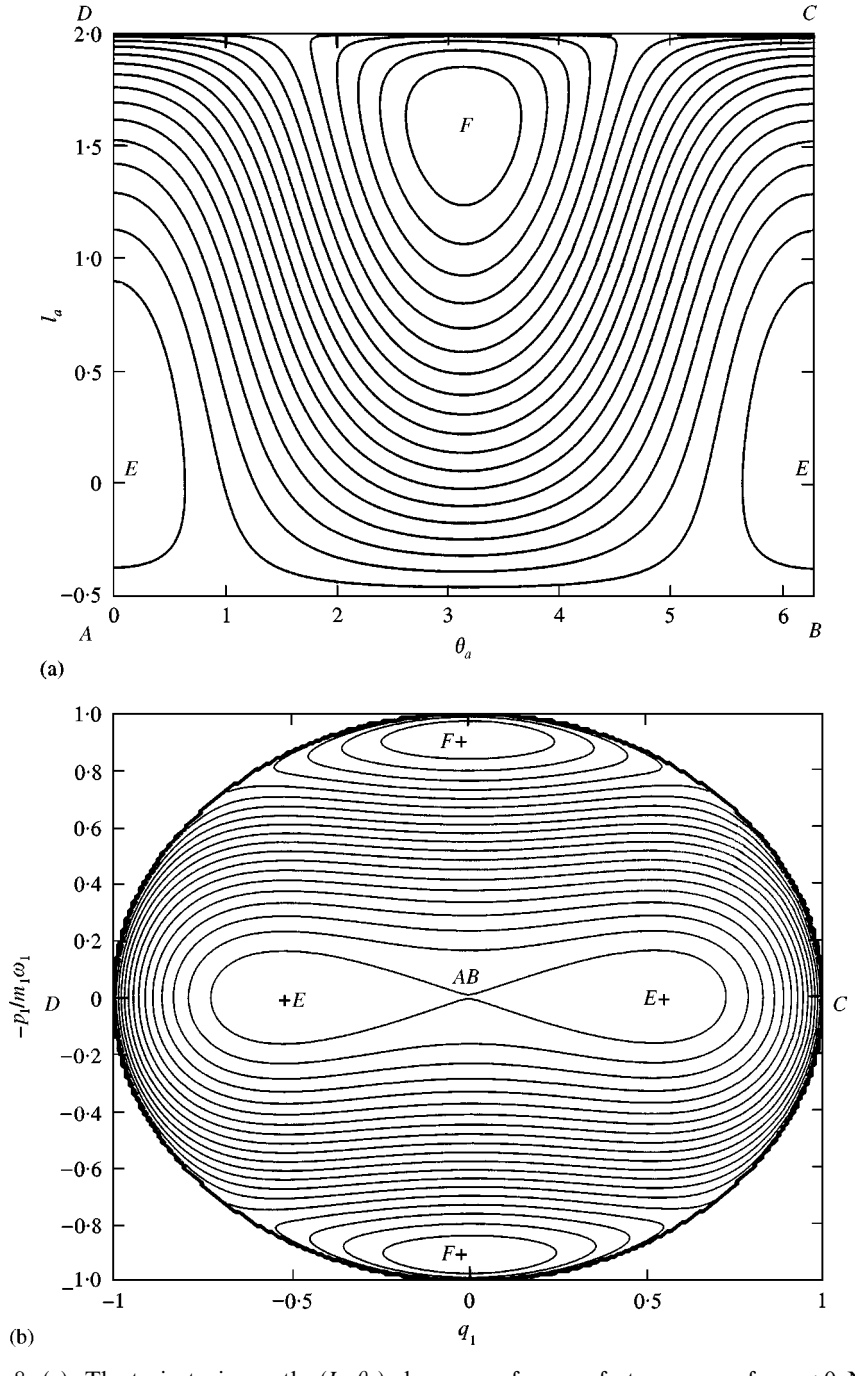

Figure 8. (a). The trajectories on the (I_a, θ_a) plane away from perfect resonance for $\varepsilon < 0$. Note the points E and F corresponding to periodic orbits have approached lines AB and CD respectively; (b) the corresponding picture on the Poincaré plane for $\varepsilon < 0$.

orbits correspond to the points of zero slope on the function $I_a\varepsilon \pm \bar{H}_{1ma}(I_a)$, and are thus given by

$$|\varepsilon| = \frac{b}{2}\frac{(-6I_a + 7I_b)}{\sqrt{(-I_a + 2I_b)}} = \frac{b}{2}\frac{(-I_1 + 4I_2)}{\sqrt{I_2}} = \varepsilon_{\text{bif}} - \frac{b}{2}\frac{I_1}{\sqrt{I_2}}$$

$$\approx \varepsilon_{\text{bif}} - \frac{b}{2}\frac{I_1\sqrt{\omega_2}}{\sqrt{\bar{H} - I_1\omega_1}}, \tag{41}$$

where the last identity has been obtained by using the small displacement approximation $\bar{H} \approx H_0 = I_1\omega_1 + I_2\omega_2$. Approaching the bifurcation (as E or F approaches the line AB, Figure 6) we have $I_1 \to 0$, and to leading order the action I_1 of the periodic orbit rises linearly with $\varepsilon_{\text{bif}} - |\varepsilon|$ from the bifurcation point. Since $I_1 = \frac{1}{2}m_1\omega_1 A_1^2$, the amplitude A_1 rises from the bifurcation as the square root of $\varepsilon_{bif} - |\varepsilon|$, giving the expected parabolic form for a period-doubling bifurcation. Figure 9 shows schematically the bifurcation diagram obtained by sweeping across a dynamic instabilility region under increasing ε. Note that the periodic orbit created at the left-hand stability boundary is not destroyed at the right-hand boundary, but continues to grow, existing outside the instability region. That it cannot be destroyed in this direction is readily seen from the function $\bar{H}_{1ma}$, where no amount of linearly additive $I_a\varepsilon$ can ever overcome the infinite slope of the square-root singularity at the $I_2 = 0$ end of the (I_a, θ_a) plane (line CD, Figure 6).

4. DYNAMIC INSTABILITY REGIONS

The concertina mode oscillation becomes unstable when its initial amplitude q_2^0 is given by equation (40). For this to occur at very small initial displacements ($q_2^0 \approx 0$) requires

$$2 - \omega_2/\omega_1 \approx 0. \tag{42}$$

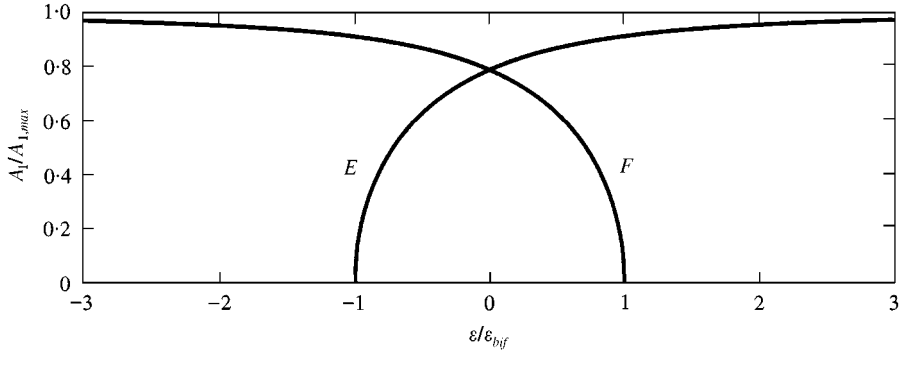

Figure 9. The bifurcation diagram through an instability region under changing detuning parameter ε, showing the birth of the periodic orbits E and F at period-doubling bifurcations on the stability boundary.

Upon defining $s = \pi R/L$ as the measure of axial wavelength, and using equation (11), this leads to

$$\left(\left(1 + \frac{n^2}{s^2}\right)^2 - 4\right)\left(\frac{\alpha^2 s^4}{3(1-\nu^2)} - \frac{1}{(1 + (n^2/s^2)^2}\right) \approx 0. \tag{43}$$

Instabilities at arbitrarily small initial displacements can therefore be obtained at critical axial wavenumbers s_1 and s_2 given by

$$s_1 = n \quad \text{and} \quad s_2 = \sqrt{\frac{\sqrt{3(1-\nu^2)}}{\alpha} - n^2}. \tag{44}$$

The former is a purely geometric criterion, and corresponds to square chequerboard panels. The second depends on shell thickness ratio and circumferential wavenumber, and (weakly) on the material (through Poisson's ratio).

In terms of the initial hoop strain ε_{hoop} of the concertina mode, the boundaries of the dynamic instability regions are given by

$$\varepsilon_{hoop}(\alpha, \nu, \mathrm{s}, n) = q_2^0 h/R = 2(2f_1 - f_2)f_1 f_3, \tag{45}$$

where

$$f_1(\alpha, \nu, s, n) = \left(\frac{\alpha^2 s^4}{12(1-\nu^2)}\left(1 + \frac{n^2}{s^2}\right)^2 + \frac{1}{(1 + (n^2/s^2))^2}\right)^{1/2}, \tag{46}$$

$$f_2(\alpha, \nu, s) = \left(\frac{4\alpha^2 s^4}{3(1-\nu^2)} + 1\right)^{1/2}, \qquad f_3(s, n) = \left(1 + \frac{8}{(1 + (n^2/s^2))^2}\right)^{-1}. \tag{47,48}$$

For, as an example, a shell with thickness ratio $\alpha = 1/400$, and Poisson's ratio 0·3, the dynamic instability region for the case with circumferential wavenumber $n = 10$ is shown in Figure 10. The initial concertina-mode hoop strain required for instability is thus extremely large (of the order of millistrain), except in the immediate vicinity of the two critical axial wavenumbers s_1 and s_2 (in this case, $s_1 < s_2$). For metal shells, feasible vibration strains are at most microstrain, and thus to experience this $n = 10$ instability, the concertina wavenumber must equal either s_1 or s_2 to impractically high precision.

However, plotting the instability regions for all possible circumferential wavenumbers, as in Figure 11, reveals that if the two critical axial wavenumbers s_1 and s_2 are close, the instability region can be comparatively broad even when the initial concertina-mode hoop strains are down at the microstrain level. This more pronounced resonance, occurring when $s_1 \approx s_2$, is observed when

$$s \approx n \approx \sqrt{\sqrt{3(1-\nu^2)}/2\alpha}. \tag{49}$$

For $\nu = 0{\cdot}3$, this gives $s \approx n \approx 0{\cdot}91/\sqrt{\alpha}$, and in Figure 11, where $1/\alpha = 400$ the most significant instability occurs as expected near $s \approx n \approx 18$. This theory therefore predicts that this resonance is most likely to be observed when there are $1{\cdot}82\sqrt{N}$ square panels of the chequerboard mode circumferentially, where $N = 1/\alpha$ is the ratio of shell radius to thickness, with one chequerboard panel corresponding to a complete wavelength of the concertina mode.

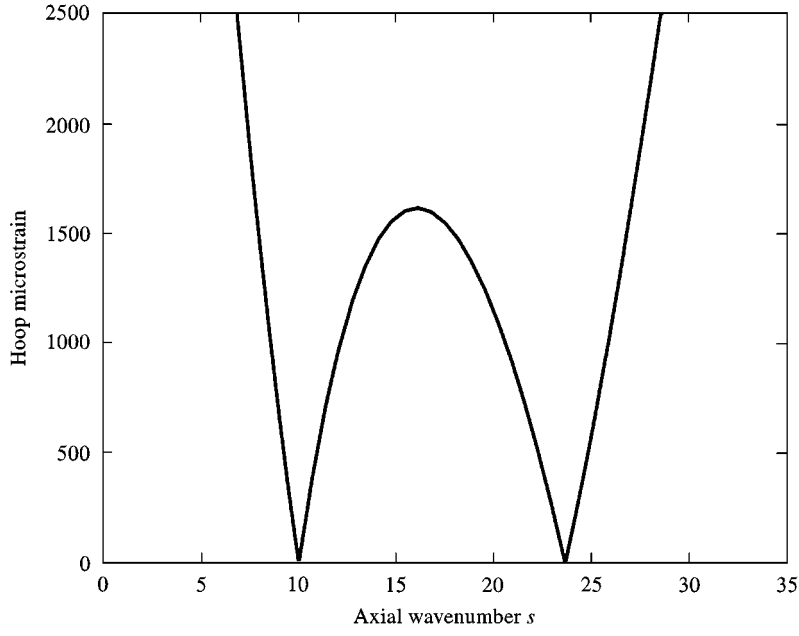

Figure 10. The instability boundary for the $n = 10$ chequerboard mode for a shell with $\alpha = 1/400$, showing two critical axial wavenumbers at which the instability occurs at arbitrarily small initial concertina mode hoop strain.

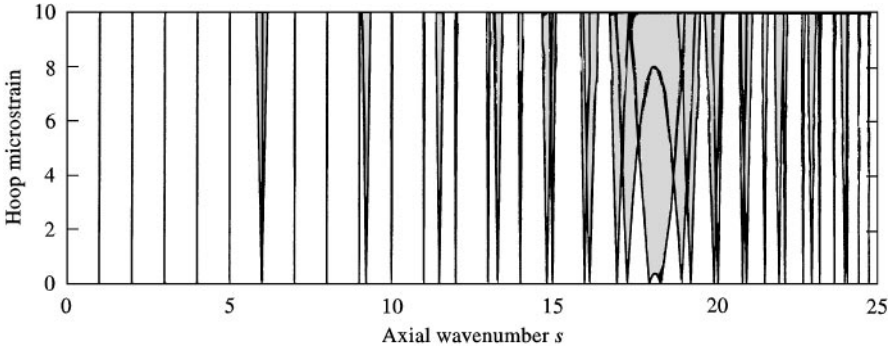

Figure 11. The instability boundaries for all possible chequerboard modes for a shell with thickness ratio $\alpha = 1/400$ and Poisson's ratio 0.3. When $n \approx 0.91\sqrt{1/\alpha} \approx 18$, the two critical axial wavenumbers are close and the W-shaped instability boundary extends over a broad range, even at very low concertina mode hoop strain.

5. CONCLUSIONS

We have applied methods of Hamiltonian dynamical stystems theory to a particular instance of modal interaction in the free, undamped vibrations of a cylindrical shell. Our primary conclusion is that the method of averaging, applied in the manner described here, leads to an elegant description of the modal interaction phenomenon. A qualitative geometrical picture of the underlying dynamics emerges which lends itself readily to the extraction of important

quantitative information, without recourse to the lengthy and *ad hoc* algebraic manipulations required by other approximation methods.

In this study we looked at the possible exchange of energy between a concertina and chequerboard mode of oscillation. Shells have many other modes of oscillation, and a host of other interaction phenomena (chequerboard–chequerboard, axial–chequerboard, etc.), are possible. However, for the particular modes considered here the theory predicts that significant exchange of energy is most likely to occur if the chequerboard panels are square, with $1{\cdot}82\sqrt{N}$ panels circumferentially, where N is the ratio of shell radius of thickness. The corresponding concertina mode will have an axial wavelength equal to one chequerboard panel, and under these conditions, initial concertina oscillations are likely to lose stability, transferring energy back and forth into the chequerboard mode oscillating at half the concertina frequency.

ACKNOWLEDGMENT

The research of AAP was supported by the Engineering and Physical Sciences Research Council of the U.K. under the Applied Non linear Mathematics Initiative.

REFERENCES

1. D. O. Brush and B. O. Almroth 1975 *Buckling of Bars, Plates, and Shells.* New York: McGraw-Hill.
2. C. R. Calladine 1983 *Theory of Shell Structures.* Cambridge: Cambridge University Press.
3. L. H. Donnell 1976 *Beams, Plates, and Shells.* New York: McGraw-Hill.
4. S. P. Timoshenko and S. Woinowsky-Krieger 1959 *Theory of Plates and Shells.* New York: McGraw-Hill.
5. N. Yamaki 1984 *Elastic Stability of Circular Cylindrical Shells.* Amsterdam: North-Holland.
6. A. S. Wolmir 1962 *Biegsame Platten und Schalen.* Berlin: Verlag für Bauwesen.
7. G. W. Hunt, K. A. J. Williams and R. G. Cowell 1986 *International Journal of Solids and Structures* **22,** 1501–1515. Hidden symmetry concepts in the elastic buckling of axially-loaded cyclinders.
8. J. G. A. Croll 1982 *Proceeding of the Institution of Civil Engineers* Part 2 **73,** 633–652. Elastic–plastic buckling of pressure and axial loaded cylinders.
9. C. P. Ellinas and J. G. A. Croll 1983 *Journal of Strain Anlysis* **18,** 41–67. Experimental and theoretical correlations for elastic buckling of axially compressed stringer stiffened cylinders.
10 D. A. Evensen 1974 *Thin-Shell Structures* (Y. C. Fung and E. E. Sechler, editors). Englewood Cliffs, NJ: Prentice-Hall. Nonlinear vibrations of circular cylindricl shells.
11. A. S. Volmir 1972 *Nonlinear Dynamics of Plates and Shells* (in Russian). Moscow: Nauka.
12. A. H. Nayfeh and B. Balachandran 1989 *Applied Mechanics Reviews* **42,** Part 2, S175-S201. Modal interactions in dynamical and structural systems.
13. D. K. Liu 1988 *Ph.D. Thesis, Technical University Delft, The Netherlands.* Nonlinear vibrations of imperfect thin-walled cylindrical shells.
14. A. Bogdanovich 1993 *Nonlinear Dynamic Problems for Composite Cylindrical Shells.* London: Elsevier.

15. J. M. T. THOMPSON and J. R. DE SOUZA 1996 *Proceedings of the Royal Society of London* **A 452,** 2527–2550. Suppression of escape by resonant modal interactions: in shell vibration and heave-roll capsize.
16. A. A. POPOV, J. M. T. THOMPSON and F. A. McROBIE 1998 *Journal of Sound Vibration* **209**, 163–186. Low dimensional models of shell vibrations. Parametrically excited vibrations of cylindrical shells.
17. B. V. CHIRIKOV 1979 *Physics Reports* **52,** 263–379. A universal instability of many-dimensional oscillator systems.
18. M. F. AUGUSTEIJN and E. BREITENBERGER 1980 *Journal of Mathematical Physics* **21,** 462–471. Integration of near-resonant systems in slow-fluctuation approximation.
19. M. F. AUGUSTEIJN and E. BREITENBERGER 1981 *Journal of Mathematical Physics* **22,** 51–66. Stability of constant-amplitude motions in slow-fluctuation approximation.
20. E. BREITENBERGER and R. D. MUELLER 1981 *Journal of Mathematical Physics* **22,** 1196–1210. The elastic pendulum: a nonlinear paradigm.
21. L. FALK 1978 *American Journal of Physics* **46,** 1120–1123. Recurrence effects in the parametric spring pendulum.
22. T. R. KANE and M. E. KAHN 1968 *Journal of Applied Mechanics* **35,** 547–552. On a class of two-degree-of-freedom oscillations.
23. M. G. RUSBRIDGE 1980 *American Journal of Physics* **48,** 146–151. Motion of the sprung pendulum.
24. E. H. DOWELL and C. S. VENTRES 1968 *International Journal of Solids and Structures* **4,** 975–991. Modal equations for the nonlinear flexural vibrations of a cylindrical shell.
25. M. V. BERRY 1987 *Hamiltonian Dynamical Systems* (R. S. MACKAY and J. D. MEISS, editors). Bristol: Adam Hilger. 1978 *American Institute of Physics Conference Proceedings* **46,** 16–120. Regular and irregular motion.
26. H. GOLDSTEIN 1980 *Classical Mechanics.* Reading, Massachusetts: Addison-Wesley.
27. V. I. ARNOLD 1989 *Mathematical Methods of Classical Mechanics.* Berlin: Springer.